



**HAL**  
open science

# **In-situ measurements of magmatic volatile elements, F, S, and Cl, by electron microprobe, secondary ion mass spectrometry, and heavy ion elastic recoil detection analysis**

Estelle F. Rose-Koga, Kenneth T. Koga, Jean-Luc Devidal, Nobumichi Shimizu, Marion Le Voyer, Célia Dalou, Max Döbeli

## ► To cite this version:

Estelle F. Rose-Koga, Kenneth T. Koga, Jean-Luc Devidal, Nobumichi Shimizu, Marion Le Voyer, et al.. In-situ measurements of magmatic volatile elements, F, S, and Cl, by electron microprobe, secondary ion mass spectrometry, and heavy ion elastic recoil detection analysis. *The American Mineralogist*, 2020, 105 (5), pp.616-626. 10.2138/am-2020-7221 . hal-02930778

**HAL Id: hal-02930778**

**<https://uca.hal.science/hal-02930778>**

Submitted on 10 Nov 2020

**HAL** is a multi-disciplinary open access archive for the deposit and dissemination of scientific research documents, whether they are published or not. The documents may come from teaching and research institutions in France or abroad, or from public or private research centers.

L'archive ouverte pluridisciplinaire **HAL**, est destinée au dépôt et à la diffusion de documents scientifiques de niveau recherche, publiés ou non, émanant des établissements d'enseignement et de recherche français ou étrangers, des laboratoires publics ou privés.

1 **High precision *in-situ* measurements of volatile F, S and Cl by electron**  
2 **microprobe, secondary ion mass spectrometry, and elastic recoil detection**  
3 **analysis: a comparative study with application to melt inclusions**

4

5 Estelle F. Rose-Koga<sup>1</sup>, Kenneth T. Koga<sup>1</sup>, Jean-Luc Devidal<sup>1</sup>, Nobumichi Shimizu<sup>2</sup>,  
6 Marion Le Voyer<sup>3</sup>, Celia Dalou<sup>4</sup>, Max Döbeli<sup>5</sup>.

7 (1) Université Clermont Auvergne, CNRS UMR6524, IRD, OPGC, Laboratoire Magmas et Volcans,  
8 F-63000 Clermont-Ferrand, France

9 (2) Woods Hole Oceanographic Institution, Dpt Geology & Geophysics, MA, USA

10 (3) Smithsonian Institution, National Museum of Natural History, PO Box 37012, MRC 119,  
11 Washington, DC 20013, USA

12 (4) Centre de Recherches Pétrographiques et Géochimiques, UMR7358, CNRS - Université de  
13 Lorraine, BP20, 54501 Vandoeuvre-lès-Nancy Cedex, France

14 (5) Laboratory for Ion Beam Physics, ETH Zürich, Zürich, Switzerland

15

16

17 **Abstract**

18 Electron probe and ion probe are the two most used instrument for *in situ* analysis of  
19 halogens in geological materials. The comparison of these two methods on widely  
20 distributed glass standards (ex: MPI-DING) is needed. We report analyses of F, S and  
21 Cl concentrations in 3 geological glass samples (EPMA) and 10 referenced standards  
22 (EPMA and SIMS). F and Cl absolute abundances have been determined  
23 independently for three of the standards (ML3B-G, ATHO-G and KE12), via elastic  
24 recoil detection analysis (ERDA), to certify the accuracy of the cross-calibration  
25 EPMA-SIMS. The detection limits for EPMA are a 150 µg.g<sup>-1</sup> for F, 20 µg.g<sup>-1</sup> for S  
26 and Cl and for SIMS < 48 µg.g<sup>-1</sup> for F, < 3 µg.g<sup>-1</sup> for S and <19 µg.g<sup>-1</sup>. On SiO<sub>2</sub>-  
27 rich glass-standards, F and Cl measurements by ERDA highlight a matrix effect

28 during SIMS analysis of F and Cl. With the ERDA independently measured value, we  
29 therefore propose an alternative calibration function to correct this matrix effect on  
30 the SIMS measurements of F, S and Cl. The application of F and Cl measurements on  
31 arc melt inclusions shows that over a wide range of H<sub>2</sub>O degassing, F/Cl remains  
32 constant for a given series of inclusions from a single volcano, suggesting F/Cl ratios  
33 are unchanged during volcanic degassing.

34

35 Keywords: F, Cl, SIMS, EPMA, ERDA, melt inclusion

36

37 Introduction

38 The behavior of trace volatile elements (magmatic volatile components other  
39 than H<sub>2</sub>O and CO<sub>2</sub>) in magmas has inspired many scientific contributions in the past  
40 decades (e.g. Baker et al., 2005; Wallace, 2005; Behrens and Gaillard, 2006; Fischer,  
41 2008; Aiuppa et al., 2009 and reference therein). For an extensive review of the  
42 interest of halogens in Earth Sciences see Hanley and Koga, 2018 (in special volume  
43 by Harlov and Aranovich, 2018 and reference therein). In short, the interests go from  
44 partition coefficients of F, Cl and S between minerals and melt or fluid (e.g. Dalou et  
45 al., 2012; Zajacz et al., 2012; Bernini et al., 2012; Wu and Koga, 2013; Van den  
46 Bleeken & Koga, 2015; Kusebauch et al., 2015; Joachim et al., 2017; Iveson et al.,  
47 2018), to tackling mantle source compositions of these elements using melt inclusions  
48 (e.g. Straub et al., 2003; Bouvier et al., 2010; Le Voyer et al., 2010; Helo et al., 2012;  
49 Rose-Koga et al., 2012, 2014, 2017; Métrich et al., 2014; Cabral et al., 2014; Hartley  
50 et al., 2014; Jackson et al., 2015a) or using glasses (e.g. Kendrick et al., 2012;  
51 2014a,b; 2015; Jackson et al., 2015b) or minerals (olivine: Broadley et al., 2019), to  
52 measuring the diffusion rate of volatile elements to assess magma ascent rates (e.g.

53 Llyod et al., 2014; Ferguson et al., 2016; Ruth et al., 2018) and assessing magma  
54 degassing (e.g. Bureau et al., 2000; Edmonds et al., 2001; Balcone-Boissard et al.,  
55 2010).

56 Bulk method for determining F and Cl contents in geological samples have improved  
57 through the years and pyrohydrolysis followed by ion chromatography have improved  
58 to reach detection limits of  $0.2\mu\text{g.g}^{-1}$  (Michel and Villemant, 2003) even  $0.1\mu\text{g.g}^{-1}$   
59 (Blacone-Boissard et al., 2009), which remains a factor of 10 to 30 better than that  
60 reported later with the same analytical tehnic by Marks et al. (2016;  $10\text{-}20\mu\text{g.g}^{-1}$  for F  
61 and  $20\text{-}30\mu\text{g.g}^{-1}$  for Cl). Here we want to compare in-situ analytical technics for F  
62 and Cl measurements because the study of smaller and smaller geological samples are  
63 requiring intercalibration and comparison of the technics to make an educated  
64 decision on which one to use to achieve the goal we have.

65 With recent advances of micro analytical techniques and melt inclusion studies, there  
66 is a growing body of concentration measurements of relatively volatile, light-atomic-  
67 mass elements (H, B, C, F, S, Cl) in MORB glasses and primitive melts of subduction  
68 zone magmas (e.g. Sisson and Layne 1993; Métrich *et al.* 1999; Hauri et al., 2002;  
69 Wade *et al.* 2006; Le Voyer *et al.* 2008, 2010; Bouvier et al., 2008; Rose-Koga *et al.*  
70 2012; see also references in Wallace 2005). Other volatile element, moderatly heavier,  
71 such as Br have also been successfully measured by secondary ion mass spectrometry  
72 (Cadoux et al., 2017). While C and H and to a lesser extend S are likely to suffer  
73 degassing (Dixon *et al.* 1995), halogens such as F and Cl (and probably Br) are often  
74 under-saturated in these primitive basaltic melts, indicating that they did not  
75 experience any degassing or fractionation event (e.g. Carroll and Webster 1994;  
76 Bucholz et al., 2013).

77 Among the difficulties contributing to the limited comparison of the preexisting data,

78 was, suprisingly, the lack of published comparison of S, Cl and F measurements of  
79 standards between the two most used *in situ* analytical procedures: electron  
80 microprobe (EPMA) and the ion probe (SIMS). Recently, a F, S and Cl comparison  
81 between literature data obtain by EPMA and by SIMS (Le Voyer et al., 2019)  
82 concluded that inter-laboratory comparisons agreed within 10% for F and to a variable  
83 degree for S and Cl, and propose a quality controlled published-data summary table  
84 (Table S2 available through the EarthChem Library,  
85 <http://dx.doi.org/10.1594/IEDA/111195>).

86 Electron microprobes perform microanalysis of volatile elements, but the high  
87 detection limits of this technique (tens to hundreds of ppm) place limitations on many  
88 volatile studies (cf. Devine *et al.* 1995 and references therein). After a study  
89 improving the F measurement by EPMA (Zhang et al., 2016), the inter-calibration of  
90 EPMA and SIMS is timely and echoes conference abstracts about this recurrent  
91 subject (e.g. Rose-Koga et al., 2008; Guggino and Hervig, 2010). This will be the  
92 basis to push further the investigations for example of the degassing processes via  
93 experimental approach and *in situ* melt inclusion studies. Also it is noted that F, S,  
94 and Cl are among elements that LA-ICPMS can not measure (for measurements of  
95 major elements in melt inclusions by LA-ICPMS and intercalibration with EPMA and  
96 SIMS, see Pettke *et al.* 2004) and therefore their *in-situ* measurements in small  
97 objects such as melt inclusions rely solely on the development of their measurements  
98 by EPMA and SIMS, and their intercalibration.

99 Volatile-rich magmas are generally those of subduction zones. The current consensus  
100 is that arc magmatism is triggered by a flux, of either a volatile-rich fluid, or a silicate  
101 melt, derived from the subducting lithosphere (*e.g.* Gill 1981; Tatsumi and Eggins  
102 1995), or a fluid somewhere between the two and termed supercritical fluid (Shen and

103 Keppler 1997; Bureau and Keppler 1999; Stalder *et al.* 2000). A large number of  
104 observations on isotopic compositions of arc lavas attest the necessity of slab flux in  
105 the constitution of lavas (e.g. Tatsumi and Eggins, 1995; Hanyu *et al.*, 2012; Narvaez  
106 *et al.*, 2018). Therefore, the nature of this flux and its interaction with solid mantle or  
107 with the subducting slab determines the element fractionation processes characteristic  
108 of this geodynamic setting (e.g. for Iwate volcano, Japan; Rose-Koga *et al.*, 2014).  
109 In this paper we measure F, S and, Cl by SIMS on a set of 6 glasses from the WHOI  
110 standard-set (ALV519-4-1, ALV1654-3, ALV1649-3, GL03-D51-3, GL07-D52-5,  
111 EN113-46D-2) to create 3 working curves. We use our 3 SIMS working curves to  
112 compare our SIMS measured values of 8 MPI DING glasses (ML3B-G, KL2-G,  
113 StHs6/80-G, GOR128-G, GOR132-G, ATHO-G, T1-G, KE12) and of 2 basaltic  
114 standards (VG2 and VG-A99) with our EPMA values. We also report independent  
115 absolute F and Cl values from elastic recoil detection analysis (ERDA) of three MPI  
116 DING glasses (KE12, ATHO-G and KL2G) which independently anchors our  
117 calibration curves. Finally, we give an example of application for EPMA and SIMS  
118 measurements of Cl and F in melt inclusions.

119

## 120 Standards and glass samples

121 All glasses and standards used have already been well documented elsewhere,  
122 and we summarize here the essential points. The set of 6 basalt samples used in this  
123 study for the SIMS analysis come from several sources (Table 1). The ALV  
124 standards are fresh basaltic glasses sampled during Alvin dives over the Famous area  
125 (ALV519-4-1: Shimizu 1998; Michael and Cornell 1998), and over the Galapagos  
126 Spreading Center 85°W (ALV1654-3 and ALV1649-3; Embley *et al.* 1988; Perfit *et*  
127 *al.* 1998). GL standards are fresh basalt glasses from the Salas y Gomez seamount

128 area (GL03-D51-3 and GL07-D52-5; Simons *et al.* 2002). EN113-46D-2 is a fresh  
129 basaltic glass from the Endeavor spreading center (Simons *et al.* 2002).

130 For the other glass samples and standards we used six basalts (KL2-G, from  
131 Kilauea volcano, Hawaii; ML3B-G from Mauna Loa Volcano, Hawaii; VG2, *aka*  
132 USNM 111240/52, from the Juan de Fuca Ridge (Jarosewich 2002); VG-A99, *aka*  
133 A99, USNM 113498/1, from Kilauea volcano, Hawaii (Jarosewich *et al.* 1979); Alvin  
134 2746-15, from 9-10°N East Pacific Rise (Bowles *et al.* 2006); Alvin 2390-5, from the  
135 Siqueiros Transform, (Sims *et al.* 2002)), one andesite, (StHs6/80-G, Mt. St. Helens,  
136 USA, Jochum *et al.* 2000), two komatiites, (GOR128-G and GOR132-G both from  
137 Gorgona Island, Jochum *et al.* 2000), a rhyolite, (ATHO-G, from Iceland, Jochum *et*  
138 *al.* 2000), a quartz-diorite, (T1-G, from the Italian Alps, Jochum *et al.* 2000), two  
139 obsidians, (Sletta, from Iceland, courtesy from O. Sigmarsson; and KE12 from  
140 Eburru, Kenya; personal communication of Malik and Bungard 1974 cited in Devine  
141 *et al.* 1984).

142

### 143 **Analytical procedures**

#### 144 *EPMA analysis*

145 Electron microprobe analyses were performed with a Cameca SX 100  
146 equipped with four wavelength dispersive spectrometers (WDS) at the Laboratoire  
147 Magmas et Volcans (Clermont-Ferrand). Major elements and volatiles were analyzed  
148 in separate analytical sessions with the following detailed conditions. Major elements  
149 in glasses were analyzed at an accelerating voltage of 15 kV, an 8 nA beam current  
150 and a 20µm defocused beam. These analytical conditions are well suited for glasses  
151 analyses; no geochemical instability (sodium loss principally) is detected even for  
152 silica rich samples (e.g. Óladóttir *et al.* 2011).

153 Chlorine, sulfur and fluorine analyses were performed at 80 nA and with a 5 to  
154 20µm defocused beam together with the trace element acquisition program proposed  
155 in the Cameca Peak Sight software. This quantification model takes into account the  
156 matrix composition of the glass to calculate the traces element concentration. ZAF  
157 data reduction was carried out by the means of the X-PHI model. The analytical  
158 standards were: natural scapolite for the ClK $\alpha$  line, fluorite for FK $\alpha$  and VG-2 glass  
159 for SK $\alpha$ . Sulfur concentration in VG-2 glass is 1340 µg.g<sup>-1</sup> ; this value corresponds  
160 to the average of a compilation of published data (Dixon *et al.* 1991; Thordarsson *et*  
161 *al.* 1996; Thornber *et al.* 2002).

162

#### 163 Sulfur and chlorine

164 Because sulfur speciation (S<sup>6+</sup> or S<sup>2-</sup>) induces changes in the SK $\alpha$  spectral position  
165 (Carroll and Rutherford 1988), prior to sulfur concentration measurement and for  
166 every sample, the SK $\alpha$  peak maximum was first located by using the regular  
167 automatic routine of the Cameca SX 100 software. Then, if the measured peak  
168 position differs from the one of the standard, the new value is changed in the analysis  
169 setup.

170 The selection of the diffraction crystals is driven by the achievements of the highest  
171 peak counts to reach very low detection limits and by looking at the region of the  
172 spectrum with no interfering peaks. Thus, chlorine and sulfur were analyzed  
173 successively by using a Large pentaerythritol (LPET) crystal.

174

#### 175 Fluorine

176 The case of fluorine is more complex. This element can be measured either  
177 with a W/Si multilayer crystal (PC1) or with a thallium acid phthalate crystal (TAP).

178 Multilayer crystal allows high precision and accuracy measurements together with  
179 low detection limits. Unfortunately, for iron-bearing minerals or glasses, the  $FK\alpha$   
180 peak is strongly overlapped by the shoulder of a strong  $FeL\alpha$  line. Different studies  
181 (Todd 1996 ; Witter and Kuehner 2004) have proposed an electron microprobe  
182 method for analyzing F in Fe-bearing minerals and glasses using multilayer crystals  
183 that overcomes the spectral interference. This method is based on the linear  
184 relationship existing between the iron concentration of fluorine-free minerals (olivine  
185 and pyroxenes essentially) and the number of counts at the  $FK\alpha$  peak position in the  
186 same fluorine-free minerals. Thus, the  $FeL\alpha$  contribution (i.e. the background) can be  
187 easily deduced and quantified from the total iron concentration of the sample and  
188 subtracted from the bulk  $FK\alpha$  peak counts. However, the calibration curve of this  
189 model is only found for the analysis of  $Fe^{2+}$ -bearing minerals. In transition metals of  
190 the first row, the L-spectra exhibit peak position shifts as a function of the oxidation  
191 state (Fialin *et al.* 2001, 2004). The omission of the self-absorption induced shift of  
192 the  $L\alpha$  peak between  $Fe^{2+}$  and  $Fe^{3+}$  could lead to the overestimation of the background  
193 counts at  $FK\alpha$  peak position and thus to an underestimation of the fluorine content.  
194 The correction method established by Witter and Kuehner (2004) should be only  
195 applied for pure  $Fe^{2+}$ -bearing minerals and glasses. In order to overcome this problem,  
196 we analyzed fluorine using TAP diffraction crystals although the detector is  
197 significantly less efficient than PC1. To improve its counting statistics (precision and  
198 detection limit), fluorine was measured simultaneously on 3 spectrometers according  
199 to the Cameca multi-spectrometers counting routine. On top of the choice of the  
200 detector, we tested  $CaF_2$  and Durango apatite standards for F calibration, and  
201 concluded that  $CaF_2$  provides generally consistent results, most likely due to known F  
202 X-ray excitation issue of apatite (Stromer *et al.*, 1993).

203

204           The challenge with traces elements analysis in glass is to find a compromise  
205 between low detection limit, i.e. the used of high beam current, long counting time,  
206 and limited beam damages. Volatile loss during the analysis is minimized through the  
207 used of a protocol derived from the CSIRO-trace routine (Robinson and Graham  
208 1992). The total counting time (peak and background) for a single analysis is 40 sec  
209 and is divided as follow: 10 sec on peak and background for chlorine and sulfur but  
210 60 sec on peak and background for fluorine (20 sec per spectrometer). Low detection  
211 limit is achieved by increasing the number of analysis on the same point, thus by  
212 improving the singal-to-noise ratio. After each analysis, the beam is shielded for 20  
213 sec allowing the sample to cool down. Total volatiles concentration is calculated from  
214 the sum of the counts from the successive iterations. With 15 kV accelerating voltage  
215 and 80 nA beam current, for a total Cl and S peak counting time of 100 sec and 600  
216 sec for F. Typical detection limits for F, Cl, and S were 150, 50 and 50  $\mu\text{g}\cdot\text{g}^{-1}$ ,  
217 respectively.

218

219 *SIMS analysis*

220 *Sample preparation for SIMS*

221           The standards are mounted in high purified indium metal (e.g. Hauri *et al.*  
222 2002; Le Voyer *et al.* 2008) in a 1 inch diameter aluminum ring, put in ultrasound in  
223 pure ethanol then in distilled water for 10 minutes, respectively. Indium is used  
224 because epoxy can contain significant amounts of volatiles that can degass during the  
225 analysis and increase the background signal. The mount is dried carefully in an oven  
226 overnight. The mount is finally gold coated before analysis and kept overnight in high  
227 vacuum (low  $10^{-8}$  torrs) until being inserted in the sample chamber.

228

229 Method

230 The measurements for the working curve calibrations were done on a set of 6  
231 glass standards (Table 1), on the ion probe Cameca 1280 of Woods Hole  
232 Oceanographic Institution (MA, USA). We used a Kohler illumination with a primary  
233 beam current of 1.5 nA Cs<sup>+</sup> primary positive beam, and negatively charged secondary  
234 ions were extracted through a nominal accelerating potential of 10 kV. Due to  
235 implantation of Cs<sup>+</sup> ions and extraction of both negatively charged secondary ions and  
236 electrons, positive charging of the sample surface must be compensated with the use  
237 of an electron flood gun which delivers electrons to the sample surface. The isobaric  
238 interference were filtered by an energy slit opening at 50 eV and the contrast aperture  
239 at the cross over was large (400 μm). The entrance and exit slits are closed to achieve  
240 a mass resolution of  $M/\Delta M=5800$ .

241 We presputtered the samples surface during 180 seconds while applying a  
242 raster of 30×30 μm. The field aperture (of 8000) corresponds to an area of 15×15 μm,  
243 is inserted into the image plane. This means that only the ions originating from the  
244 central 15 μm of the flat-bottomed sputtered-crater are admitted into the mass  
245 spectrometer. The elimination of stray ions sputtered from the crater walls and  
246 desorbed from the sample surface results in very low volatile backgrounds (routinely  
247 about 0.05–0.1 counts per second for the counting system at half mass positions with  
248 the primary beam and the electron gun on). We counted 8 sec on <sup>19</sup>F, 5 sec on <sup>30</sup>Si, 5  
249 sec on <sup>32</sup>S and 8 sec on <sup>35</sup>Cl. One analysis was composed of 2 blocks of 10 cycles and  
250 took less than 15 min per spot. Intensities of <sup>19</sup>F, <sup>32</sup>S and <sup>35</sup>Cl were collected  
251 cyclically by an electron multiplier, processed through pulse-counting electronics and  
252 normalized to <sup>30</sup>Si for concentration calculations.

253

## 254 Calibration

255 Earlier studies that have involved  $\text{Cs}^+$  beam were performed on small format  
256 SIMS (Cameca 6f, Hauri *et al.* 2002). But hydride interferences, such as  $\text{SH}^-$ , are  
257 difficult to effectively eliminate using the energy filtering technique (Shimizu *et al.*  
258 1978) available on small format Cameca instruments (e.g., IMS 3f/4f/5f/6f). The high  
259 mass resolution of the SIMS 1280 of WHOI is required to eliminate the  $^{34}\text{S}^1\text{H}$   
260 interference on  $^{35}\text{Cl}$  (MRP>5120) without giving up transmission significantly (Fig.  
261 1c). The SIMS calibration curves for F, S and Cl are shown in Fig. 2. They are  
262 regressions of ion probe signals (x-axis) compared to known EPMA concentrations  
263 (y-axis). The former is the intensity ratio of two elements times the  $\text{SiO}_2$   
264 concentrations of each standards, the numerator of the ratio being the element of  
265 interest and the denominator is a matrix element common to all samples (e.g.  
266  $^{19}\text{F}/^{30}\text{Si}$ ). Typically, here  $^{19}\text{F}$ ,  $^{32}\text{S}$  and  $^{37}\text{Cl}$  are normalized against  $^{30}\text{Si}$ . This provides a  
267 robust analysis little influenced by primary beam fluctuations or by ionization  
268 efficiency changes owing to matrix effects (Shimizu and Hart, 1982). In fact, the  
269 calibrations for F, S and Cl are free of significant matrix effects. The calibration curve  
270 is determined at the beginning and at the end of each session to assure no significant  
271 drift has taken place.

272

## 273 Detection limit

274 With the calibration curves of the standards, one usually attributes the Y-  
275 intercept of the linear regression to the detection limit (*e.g.* Ihinger *et al.* 1994). This  
276 methods is not accurate enough and depends on the uncertainties of the regressed  
277 data, the leverage of the data for the higher concentrations being potentially

278 unreasonable. Ideally, only the measurements of standards with F, S, and Cl  
279 concentrations lower than the expected background can give the detection limit (see  
280 Koga et al., 2003, for this procedure during low hydrogen concentration  
281 measurements by SIMS). It was not a simple task to verify ppm-level abundance, and  
282 we adapted calibration without explicitly identifying zero point count rate (Table 1).  
283 Some studies have used adapted “blank” material such as San Carlos olivine and  
284 synthetic forsterite (Hauri et al. 2002, Le Voyer et al. 2017). With what was available  
285 to us we calculated detection limits 48  $\mu\text{g.g}^{-1}$  for F, 3  $\mu\text{g.g}^{-1}$  for S and 19  $\mu\text{g.g}^{-1}$  for  
286 Cl (Fig. 2). These values are close to the zero intercept and considering the error on  
287 the y-intercept is as large as the value itself, the linear regression of the calibration  
288 curve is equivalent to forcing the regression through zero. The slopes between forcing  
289 the linear regression through zero (red curve Fig. 2) and classic linear regression (blue  
290 curve Fig. 4) is identical within error. A detection limit of  $<1 \mu\text{g.g}^{-1}$  for F, S, and Cl  
291 was previously reported with a 6f ion probe (Hauri et al. 2002;  $<2 \mu\text{g.g}^{-1}$  for F;  
292 Guggino and Hervig 2010). With a 1280 ion probe detection limits down to 0.2  $\mu\text{g.g}^{-1}$   
293 1 for S and Cl, and 0.1  $\mu\text{g.g}^{-1}$  for F can be achieved with blank standards (Le Voyer  
294 et al., 2019). Our analytical standard error ( $\sigma$  over the 20 cycles) was typically 0.6 %  
295 for F, S and Cl (1% Le Voyer et al., 2019) and the reproducibility on the standards  
296 (2RSD) was 6.3, 3.5 and 5.2%, respectively (n=14, ALV519-4-1; comparable to 5.8,  
297 7.6 and 10.8%, respectively, on in-run standard glass P1326-2, Helo et al., 2011; 7, 4  
298 and 7%, respectively on glass VG2, Le Voyer et al., 2019).

299

### 300 *Elastic Recoil Detection Analysis (ERDA)*

301 ERDA is an absolute measurement independent from the two previous  
302 methods (EPMA and SIMS). Absolute because it consists of a shock between the

303 nuclei of 2 atoms and the radii of the two nuclei (for example  $^{19}\text{F}$  and  $^{127}\text{I}$ ) are known  
304 with great precision, and therefore the ERDA method do not require any standard to  
305 perform a measurement. ERDA has previously been used to measure hydrogen in  
306 geological materials (e.g. Mosbah et al., 1990; Bureau et al., 2009) or to intercalibrate  
307 with infrared spectroscopy measurements (e.g. Aubaud et al., 2009; Withers et al.,  
308 2012). The ERDA were made at ETH Zurich, in the Ion Beam Physics laboratory of  
309 the Paul Scherrer Institut. We used a primary ion beam of heavy ion  $^{127}\text{I}$  at 12 MeV.  
310 This iodine beam was produced by EN-tandem accelerator via cesium (Cs) sputtering  
311 of AgI. For lower projectile energies Time of Flight-ERDA (ToF-ERDA) is a widely  
312 used technique. The analytical protocol is only briefly explained in the following, full  
313 details can be found in C. Kottler *et al.* 2006 (and reference therein). The beam hits  
314 the polished plane of the sample with a low angle and the scattered element of choice  
315 (F and Cl, here) are detected by the ToF-ERDA dectector at the fixed angle of  $36^\circ$ .  
316 The recoil masses are identified by means of a coincident measurement of the particle  
317 velocity and total energy. The recoil energy for  $^{19}\text{F}$  is 3.5 MeV and that of  $^{35}\text{Cl}$  is 5.3  
318 MeV. Here a gas ionization chamber (GIC) instead of silicon detectors has been used  
319 for energy measurements because silicon detectors suffer from considerable radiation  
320 damages. This standard-free method gives absolute F and Cl concentrations. The  
321 shape of the beam on the sample is a rectangle of  $1\text{ mm} \times 4\text{ mm}$  but only a small part  
322 of it was actually targeting the sample, the rest was hitting the surrounding indium. A  
323 classical ERDA graph displays a time of flight curve for each ion versus energy  
324 (Kottler *et al.* 2006). These curves are processed to extract a spectrum for each  
325 elements (Fig. 3a, b, c)

326

327 **Results**

328 There is a good general agreement on mafic standards for the measurements of F, S  
329 and Cl between EPMA and SIMS above a certain threshold of concentrations, >150  
330  $\mu\text{g}\cdot\text{g}^{-1}$  for F, and >20  $\mu\text{g}\cdot\text{g}^{-1}$  for S and >20  $\mu\text{g}\cdot\text{g}^{-1}$  for Cl (Fig. 4). For  $F < 150 \mu\text{g}\cdot\text{g}^{-1}$   
331 SIMS can measure differences in F concentrations with a precision better than 10%  
332 relative when EPMA has a precision equal to the measured value (Fig. 4a). The  
333 performance of both EPMA and SIMS are in excellent agreement for Cl  
334 measurements down to 20  $\mu\text{g}\cdot\text{g}^{-1}$  (Fig. 4c). But for S measurements, SIMS can  
335 measure S concentrations below 10  $\mu\text{g}\cdot\text{g}^{-1}$  when EPMA will not measure resolvable  
336 difference in standards with  $S < 10 \mu\text{g}\cdot\text{g}^{-1}$  (Fig. 4b).

337 The glass standards measured here have reported value that can vary up to a factor of  
338 10 for certain elements (ex: Cl in StHs6/80; Table 2). Nonetheless, overall we note  
339 that technical improvement of in-situ instruments make it possible to reach  
340 interlaboratory agreements. Our EPMA and SIMS measurements most of the time  
341 agree within error with the reported values published since 2006 (ex: Jochum et al.,  
342 2006), simply improving the precision in some cases. When they do not agree, we can  
343 invoke millimeter scale heterogeneity of the standards. They have been reported for  
344 trace elements in the ATHO-G rhyolite (MPI-DING; Borisova et al., 2010) and  
345 cautious must apply when choosing your standards to perform micro-analysis. For  
346 example it is clear from Table 2 that the ATHO-G piece that we have is very different  
347 than the piece measured by SIMS in Jochum et al, 2006, and much closer to the  
348 composition of that of Oskarsson et al. (1982) and this has nothing to do with the  
349 quality of the analysis. In this respect, ATHO-G and StHs6/80-G appears to be  
350 heterogenous for F, S and Cl depending on the pieces you have. Also the  $2\sigma$  error we  
351 report for our EPMA are 9 times out of 10 better than previously reported,

352 demonstrating that the proposed settings for halogen measurements by EPMA are  
353 particularly well suited.

354 The ERDA results for F and Cl in ATHO-G, KE12 and KL2-G anchors independently  
355 the calibration curves for F and Cl. We note that the ERDA values for F and Cl of the  
356 two SiO<sub>2</sub>-rich standards, are closer to the EPMA values than the SIMS values (Fig. 4a  
357 and 4c), and the ERDA measurement on the basalt standard KL2-G was difficult to  
358 assess because of the high detection limit of the ERDA.

359

## 360 **Discussions**

### 361 *Precision and accuracy*

362 The lowest concentrations we measured were samples GOR-128 and GOR-  
363 132 for F and S and sample StHs for Cl (Table 2). While EPMA measurements tend  
364 to level out around 10 µg.g<sup>-1</sup> concentration for S (Fig. 4b), SIMS measurements are  
365 precise to µg.g<sup>-1</sup> level for S and Cl (Fig.4b and c). For F, S and Cl, SIMS  
366 measurements always display smaller error bars (Fig. 4a, b, c). Samples with  
367 concentration in S, Cl > 100 µg.g<sup>-1</sup> are analyzed with similar precision with both  
368 methods. Measurements of F remains up to 5 times more precise with SIMS than  
369 EPMA on the basis of analytical precision based on counting statistics and for F  
370 concentration above 100 µg.g<sup>-1</sup>. Because many standard values are still tied to EPMA  
371 measured samples, it appears that the uncertainty of the slope and intercept (Fig. 2)  
372 contributes to the final uncertainty similar to EPMA values (Table 2). Therefore, it is  
373 strongly recommended to use SIMS when the interest of measurement is to detect  
374 variations of concentration among similar samples with a high precision, while EPMA  
375 can certainly provide a rapid, good assessment of trace volatile abundances above a  
376 certain threshold.

377

378 *Matrix effect*

379 It is particularly notable that some measure values by SIMS (reported for ATHO-G  
380 and KE12; Table 2) significantly differ from those of EPMA and ERDA. Fig. 4 also  
381 shows that higher SiO<sub>2</sub> glasses (e.g. ATHO and KE12) plot on the right side of the  
382 1:1 line, outside of +/-20 % bound (a conservative external reproducibility range),  
383 indicating SIMS measurements are higher than EPMA and ERDA. While such offset  
384 is not present for mafic glasses which have similar SiO<sub>2</sub> content as the calibration  
385 standards. This offset is present for measurements of F, S and Cl. This systematic  
386 disparity related to the composition of material analyzed is called matrix effect, in  
387 which the secondary ion emission is influenced by change either structural or  
388 compositional variation of the matrix.

389 The relative sensitivity factor (RSF) describes a bias of an elemental ratio introduced  
390 by SIMS:  $RSF = (C_i/C_{ref}) \times (I_{ref}/I_i)$ , where  $C_i$  and  $C_{ref}$  are the known atomic  
391 concentration of mass  $i$  and mass  $ref$ , respectively and  $I$  denotes the measured signal  
392 intensity. Essentially, the slope of the calibration function is a representative RSF of  
393 several calibration standards. It should be noted that RSF cannot distinguish bias of  
394 the signal of interest (e.g.  $I_F$ ,  $I_S$ , and  $I_{Cl}$ ) from the signal of reference ( $I_{Si}$ ). Fig. 5 shows  
395 the value of RSF calculated for the samples of Fig. 4 as a function of SiO<sub>2</sub>, excluding  
396 the EPMA data below detection limit. It appears that RSF is slightly negatively  
397 correlated against SiO<sub>2</sub>, consistent with a presence of matrix effect for the high SiO<sub>2</sub>  
398 samples. However, considering the scatter of RSF values, the apparent negative  
399 correlation has only slight statistical significance. The data acquired here is not  
400 sufficient to discern the exact role of the “matrix effect”. Because of such tendency,  
401 van den Bleeken and Koga (2015) concluded from a similar analysis that as a first

402 order, one should be able to approximate the abundance of these element without  
403 correction.

404

#### 405 *Choices of calibration method*

406 Reference mass: concentration analysis by SIMS requires a ratio of the element of  
407 interest (F, S, Cl here) over an element that constitute the matrix. For silicate glasses,  
408 it is commonly Si is chosen (Shimizu and Hart).  $^{30}\text{Si}$  is commonly selected for its low  
409 abundance permitting the use of electron multiplier detector. However, depending on  
410 the SIMS facility, different reference mass is used. For example,  $^{28}\text{Si}$  detected with  
411 Faraday cup can be used as the reference mass, as well as  $^{18}\text{O}^-$  or  $^{16}\text{O}^-$ . In general,  
412 emission of negative oxygen atom is approximately 10 times better than Si but this  
413 does not seem to result in significantly more stable signal. While it will require  
414 further study to assess the advantages and disadvantages regarding the choices of the  
415 reference mass, a comparison results from different SIMS labs concluded that it  
416 would not influence the measurement significantly (in the electronic supplement, van  
417 den Bleeken and Koga, 2015).

418 Calibration curves: a linear function that converts a SIMS intensity ratio to a  
419 concentration can be expressed in following two ways.

$$420 [\text{F, S, Cl ppm}] = \text{Coef} \times (\text{I}(\text{F, S, Cl}) / \text{I}(\text{Si})) \times [\text{SiO}_2] + \text{Intercept} \quad (\text{eq. 1})$$

$$421 [\text{F, S, Cl ppm}] = \text{Coef} \times (\text{I}(\text{F, S, Cl}) / \text{I}(\text{Si})) + \text{Intercept} \quad (\text{eq. 2})$$

422 where, brackets indicates concentration and  $\text{I}(x)$  indicates SIMS intensity (i.e. count  
423 rate) of mass  $x$ . Coef, and Intercept are constants determined by fitting the function  
424 using known concentration standards. Among SIMS measurements reported, these  
425 two equations were commonly used. The eq. 2 is sufficient for the measurement with  
426 a good match of sample and standard matrices (i.e. similar  $\text{SiO}_2$  content). In the

427 current study, we adapted eq. 1, which corrects for variable SiO<sub>2</sub> content (e.g. 50%  
428 basalt and 70% rhyolite). However, it should be noted that the eq. 1 does not correct  
429 for the matrix effect.

430 Recognising the weak correlations between SiO<sub>2</sub> and RSF, we have explored a  
431 potential modification of the working curve function in an aim to optimize the  
432 accommodation of SiO<sub>2</sub> variation in silicate glass. Taking Cl as an example, the eq. 1  
433 can be rearranged to show the relationship with RSF.

$$434 \frac{[Cl] - [Intercept]}{[SiO_2]} \times k = RSF \times (I_{Cl}/I_{Si}) \quad \text{eq. (1')}$$

435 Where k is a conversion factor for concentration ratio to atomic ratio, thus Coef =  
436 RDF/k. Inspecting Fig. 5, we decided to explore two functional forms relating RSF  
437 and SiO<sub>2</sub>.

$$438 RSF = a / [SiO_2] + b \quad \text{(eq. 3)}$$

$$439 RSF = c \times [SiO_2] + d \quad \text{(eq. 4)}$$

440 Substituting eq. 3 or eq. 4 into eq. 1', the working calibration curve will be in  
441 following form.

$$442 [Cl] = ak(I_{Cl}/I_{Si}) + bk(I_{Cl}/I_{Si})[SiO_2] + Intercept \quad \text{(eq. 5)}$$

$$443 [Cl] = dk(I_{Cl}/I_{Si})[SiO_2] + ck(I_{Cl}/I_{Si})[SiO_2]^2 + Intercept \quad \text{(eq. 6)}$$

444 Table 3 shows the result of regression with above equations. For the regression, in  
445 addition to six calibration standards, three high Si samples are added T1g, ATHO, and  
446 KE12. Inspecting the results of the regression, eq. 6 consistently produced better fit,  
447 although slight, than eq. 5. On top of this, 'ck' term is significantly smaller than 'dk'  
448 term in eq. 6. This suggest that the role of additional term in correcting the matrix-  
449 dependent calibration is minor. This conclusion is again consistent with that of van  
450 den Bleeken and Koga (2015) in which authors concluded the use of eq. 1 is sufficient  
451 to determine trace halogen concentration in a wide range of silicate glasses. Lastly,

452 recalculated concentration using eq. 6 is presented in Table 2, indicated as SIMS [eq.  
453 6].

454

#### 455 **Applications to arc lava olivine-hosted melt inclusions**

456 Subduction zones have generally volatile-rich magmas. The magmas are produced by  
457 mantle wedge melting induced by slab-derived fluids. Lava erupting from arc these  
458 volcanoes are at least partially degassed. Olivine hosted-melt inclusions found in  
459 these lavas, are silicate droplets trapped in a host-mineral (olivine here) are less  
460 affected by degassing, and shielded from interaction with their surrounding in the  
461 magma chamber and during magma ascent. Especially for the halogens Cl and F, at  
462 pressure and temperature conditions of melt inclusion formation, they are less prone  
463 (1) to degassing (if at all) than H<sub>2</sub>O (e.g. Carroll and Webster, 1994; Métrich and  
464 Wallace, 2008), (2) to diffusing through the host-olivine (e.g. Bucholz et al. 2013;  
465 Lloyd et al. 2013; Le Voyer et al. 2014). Recent experimental results have  
466 determined F and Cl partition coefficients between melt and crystals (Dalou et al.,  
467 2014) and put forward that the large variation of F/Cl in arc melt inclusions resulted  
468 from the composition, the amount of slab agent and the degree of melting.

469 Our recent melt inclusion data combined with literature data show that although F/Cl  
470 ratios in arc melt inclusions can vary between 0.1 and 4 (see fig 5A in Dalou et al.,  
471 2014), within each sample suite, for each volcano, F/Cl is relatively constant, over a  
472 range of H<sub>2</sub>O abundance (Fig. 6). The F/Cl is normalized to the average F/Cl of each  
473 arc, so that all constant F/Cl ratio gather around the unity value. This illustrates that  
474 while H<sub>2</sub>O can vary due to degassing prior to (or after) the entrapment of melt  
475 inclusions, pre-entrapment F/Cl values remain constant. The same conclusion can be  
476 drawn with F/Cl plotted against CO<sub>2</sub>, F, or Cl. This systematics demonstrate either 1)

477 F and Cl remain in melt during degassing, a conclusion reached for example by  
478 Bucholz et al., (2013) or 2) partitioning of F and Cl between fluid and magma is  
479 identical (Wu and Koga, 2013; Dalou et al., 2014). While we focus on the  
480 incompatible behaviors of Cl and F in basaltic melt, it should be noted that there  
481 exists a number of studies and experimental work concerning Cl and F behavior in  
482 evolved magmas, with specific application to volcanology and ore deposit formations  
483 (e.g. Webster, 1990, 1992; Brenan, 1993; Giordano et al., 2004). Their results on  
484 halogen partitioning in fluid - evolved melt systems show that Cl and F are strongly  
485 partitioned into the fluid at crustal degassing conditions (Webster et al., 2018; Dolejs  
486 and Zajacz, 2018). But even if the halogens appear to degas during magmatic  
487 evolution in mid-to- shallow crust, Cl and F in primitive basalts, especially in melt  
488 inclusions, appear to retain the information of magma genesis (Koga *et al.* 2009;  
489 Bucholz et al., 2013; Rose-Koga et al., 2012, 2014) along with other lithophile trace  
490 elements (such as REE). The subduction input/output mass balance calculations show  
491 that nearly 100% of Cl coming in subduction is incorporated in arc magmatism,  
492 compared to only about 50% of F (e.g. Straub and Layne 2003; Wallace 2005).  
493 Therefore Cl and F are ideal tracers to identify the fractionation process between the  
494 slab and the flux originating from it, especially since they are scarcely present in the  
495 mantle (F reservoirs, see for example Koga and Rose-Koga, 2016; 2018). It is  
496 generally considered that Cl shows an affinity to volatile-rich fluid and F shows an  
497 affinity to silicate melt (e.g. Schilling *et al.* 1980). An experimental study on F  
498 fractionation between aqueous fluid and mineral at pressures and temperatures  
499 relevant to subduction zone settings, demonstrated for example the strong affinity of F  
500 for the silicate phase (Wu and Koga, 2013).

501 Studies of halogens in magmatic products cover a wide range of applications. Studies  
502 involving F and Cl measurements (and their ratios with trace elements) on arc  
503 samples are able to decipher the transport vector (melt and/or fluid) from slab to  
504 surface (e.g. Rose-Koga et al., 2014). Also F and Cl measurements combined with Pb  
505 isotopes can bring new constraints on the source of OIB lavas (e.g. Peterson et al.,  
506 2014) or on the volatile contents of the mantle endmembers (e.g. Rose-Koga et al.,  
507 2017). Halogens combined with Sr isotopes can decipher between mantle source Cl-  
508 enrichment and brine assimilation (e.g. Reinhardt et al., 2018)

509

### 510 **Implications**

511 F and Cl measurements by EPMA and SIMS have a general good agreement on  
512 standards glasses available to the scientific community (MPI-DING, Jochum et al.,  
513 2006). These are the two most common instruments for *in situ* halogen measurements  
514 and finally their performance are analysed and compared. The F and Cl ERDA  
515 measurements on 3 standards anchors independently the EPMA-SIMS comparison  
516 curves and gives absolute F and Cl concentrations for these standards. The ERDA  
517 results also highlight the fact that there is a matrix effect on SIMS measurements of F  
518 and Cl in high-SiO<sub>2</sub> standard. We propose a new equation to correct this matrix effect  
519 in the SIMS F and Cl data of high-SiO<sub>2</sub> samples.

520 We can now use, indifferently EPMA or SIMS for F and Cl measurements, on a large  
521 SiO<sub>2</sub> range covering most of the geological samples.

522

### 523 **Conclusions**

524 An intercalibration of F, Cl and S measurements between EPMA and SIMS is  
525 reported for 10 glass-standards. Both analytical methods are in excellent agreement

526 for standards with concentrations in these volatiles elements above 150  $\mu\text{g.g}^{-1}$  for F  
527 and above 20  $\mu\text{g.g}^{-1}$  for S and Cl. However, SIMS has a lower detection limit and is  
528 preferable in the case of low concentration samples. The ERDA measurements  
529 independently confirms and anchors our data. This study revealed a shift between  
530 acidic and mafic glass-standard on our ERDA data, thus requiring (1) cautious in the  
531 choice of standard materials, and (2) separate SIMS calibrations with standards  
532 covering the  $\text{SiO}_2$  range of the samples. An alternative is to use the equation 6 that we  
533 propose to account for this matrix effect on the SIMS measurements of F, S and Cl. In  
534 arc melt inclusions, F/Cl ratios of series of inclusion from single volcanoes, remain  
535 constant over a large range of  $\text{H}_2\text{O}$  concentration, suggesting these halogen do not  
536 degass. On a broader point of view, halogens such as F and Cl (also Br and I),  
537 associated with radiogenic isotopes and trace element ratios, are promising new  
538 tracers of fluid and/or melt transport from their source regions and for degassing  
539 processes.

540

541

542 Acknowledgement: EFR-K thank O. Sigmarsson for the Sletta sample. EFR-K and  
543 KTK acknowledge support from Region Auvergne Rhone Alpes (SCUSI program).

544 This is Laboratory of Excellence *ClerVolc* contribution number xxx.

545

546 Figure caption

547

548 Fig. 1: Secondary ion spectra at nominal masses, 19 (a), 32 (b) and 35 (c) for a basalt  
549 glass (ALV519-4-1) to illustrate the resolution of isobaric interferences at  
550  $M/\Delta M=5800$  (10% definition). This basalt glass contains  $90 \mu\text{g.g}^{-1}$  F,  $950 \mu\text{g.g}^{-1}$  S,  
551 and  $45 \mu\text{g.g}^{-1}$  Cl (Helo et al., 2011; Table 1).

552

553 Fig. 2: SIMS calibration curves for abundances of (a) fluorine, (b) chlorine, (c) sulfur  
554 in basalt glasses. The lines correspond to different fit. The red line is a linear  
555 regression line forced through zero, the blue line is a classic linear regression line, the  
556 y-intercept giving the detection limit of the analyzed element. Since any of those fit  
557 are satisfactory within the error bar, we consider the calibrations are linear over  
558 several orders of magnitude in S, Cl, F concentrations.

559

560 Fig. 3: Elastic recoil detection analysis (ERDA) spectra for oxygen  $^{16}\text{O}$  (a), fluorine  
561  $^{19}\text{F}$  (b) and chloride  $^{35}\text{Cl}$  (c). On the y-axis are reported the counts and on x-axis, the  
562 mass. This is the example of the measurements done on the standard MPI-DING glass  
563 KE12 (Jochum et al., 2006).

564

565 Fig. 4: concentrations of F (a), S (b) and Cl (c) measured by SIMS versus that  
566 measured by EPMA (circles) and ERDA (square, when applies) in a log-log plot.  
567 Standards are categorized according to their  $\text{SiO}_2$  contents into mafic, intermediate  
568 and acidic.

569

570 Fig. 5: RSF (the relative sensitivity factor) is plotted against SiO<sub>2</sub> concentration in  
571 glass samples. RSF is determined for individual analysis of known samples. (a) RSF  
572 of fluorine, (b) of sulfur, and (c) of chlorine are shown here. There exist a slight  
573 negative slope for all the panels however due to scatter of measurements, the trend is  
574 not statistically significant. There are less number of RSF values as many of sulfur  
575 concentrations are below EPMA detection limit and there were no independent way to  
576 verify their concentrations.

577

578 Fig. 6: F/Cl ratio normalized to the average versus H<sub>2</sub>O concentrations in wt%.  
579 Symbols are for olivine-hosted melt inclusions from different arcs (Sommatà: Rose-  
580 Koga et al., 2012; Ecuador: Le Voyer et al., 2008; Narvaez et al., 2018; Shasta: Le  
581 Voyer et al., 2010; Mariana: Shaw et al., 2012; Lesser Antilles: Bouvier et al., 2008,  
582 2010; Vanuatu: Sorbadère et al., 2011).

583

584 Tables

585 Table 1: F, S, Cl and SiO<sub>2</sub> measurements in 6 basalt glasses with the corresponding  
586 analytical methods and references. They are the glass-standards used for the  
587 calibration on the WHOI SIMS.

588 Table 2: Report of F, Cl, S and SiO<sub>2</sub> concentration measurements in 10 referenced  
589 material (\*) and 3 other basaltic glasses ( $\pm$  is  $2\sigma$ ). Analytical methods and references  
590 are specified.

591 Table 3: Result of error weighted regression of Eq. 5, and Eq. 6

592

593

594

595

596

597

598

599

600

601

Table 1: F, S, Cl and SiO<sub>2</sub> measurements in 6 basalt glasses with the corresponding analytical methods and references. They are the glass-standards used for the calibration on the WHOI SIMS.

	F	±	S	±	Cl	±	SiO <sub>2</sub>	Mehod; Reference
	[ppm]		[ppm]		[ppm]		wt%	
ALV519-4-1	90	30	950	95	45	23	48.9	EPMA; [1]
ALV1654-3	997	150	1562	78	2914	146	56.7	EPMA; [1], [2]
ALV1649-3	445	67	1640	82	1433	72	51.5	EPMA; [1], [2]
GL03-D51-3	299	45	1126	57	182	18	49.5	EPMA; [1], [3]
GL07-D52-5	431	65	1183	59	322	32	48.6	EPMA; [1]
EN113-46D-2	124	37	877	88	45	23	49.5	EPMA; [1], [3]

[1] Helo et al., 2012; [2] Michael & Cornell, 1998; [3] Simons et al. 2002.

Relative analytical error for F concentration >200 ppm is 15% and F<200 ppm is 30%.

Relative analytical error for S concentration > 1000 ppm is 5% , between 100 to 1000 ppm is 10% and < 100 ppm is 50%.

Relative analytical error for Cl concentration >400 ppm is 5%, between 50 and 400 ppm is 10%, and Cl< 50 ppm is 50%.

Errors of these standards are assessed on the long term reproducibility.

SiO<sub>2</sub> was measured by EPMA

Table 2: Report of F, Cl, S and SiO<sub>2</sub> concentration measurements in 10 referenced material (\*) and 3 other basaltic glasses ( $\pm$  is  $2\sigma$ ). Analytical methods and references are specified.

	F	$\pm$	S	$\pm$	Cl	$\pm$	SiO <sub>2</sub>	Method; Reference
	[ppm]		[ppm]		[ppm]		wt%	
ML3B-G*	70	18	1.2	0.12	7.5	1.4	51.4	SIMS; [1]
			100	100	110	33		EPMA; [1]
			30	30	60	18		EPMA; [1]
	64;57;69	30;20;30						EPMA; SIMS; PIGE; [2]
	71	14	5.2	0.1	36	1		SIMS; [WHOI this study]
	<b>61</b>	<b>11</b>	<b>5.1</b>	<b>0.2</b>	<b>32</b>	<b>2</b>		<b>SIMS; [eq. 6, this study]</b>
48	68	17	13	<b>32</b>	<b>21</b>	<b>50.7</b>	<b>EPMA; [LMV this study]</b>	
StHs6/80-G*	320	32	2.7	0.3	184	18	63.7	SIMS; [1]
			40	40	210	42		EPMA; [1]
					230	69		EPMA; [1]
	139;122;155	2;2;2						EPMA; SIMS; PIGE; [2]
	<d.l.		4.3	0.1	27	0.6		SIMS; [WHOI this study]
	<d.l.		<b>4.1</b>	<b>0.2</b>	<b>24</b>	<b>0.8</b>		<b>SIMS; [eq. 6, this study]</b>
28	35	19	1	<b>21</b>	<b>11</b>		<b>EPMA; [LMV this study]</b>	
T1-G*	321	32	2.6	0.3	113	14	58.6	SIMS; [1]
			30	30	100	50		EPMA; [1]
					130	65		EPMA; [1]
			0.92		119			LA-ICPMS; [3]
			1.94					LA-ICPMS; [3]
	107;94;119	6;6;8						EPMA, SIMS, PIGE; [2]
274	39	6.0	0.2	175	8		SIMS; [WHOI this study]	
<b>207</b>	<b>29</b>	<b>5.7</b>	<b>0.2</b>	<b>135</b>	<b>14</b>		<b>SIMS; [eq. 6, this study]</b>	
154	47	20	8	<b>158</b>	<b>7</b>	<b>57.5</b>	<b>EPMA; [LMV this study]</b>	
GOR128-G*	25	3	4.3	0.4	11.7	1	46.1	SIMS; [1]
			30	30	50	35		EPMA; [1]
					40	50		EPMA; [1]
	<d.l.		8.3	0.2	38	0.9		SIMS; [WHOI this study]
	<d.l.		<b>8.4</b>	<b>0.3</b>	<b>33</b>	<b>1.7</b>		<b>SIMS; [eq. 6, this study]</b>
4	8	15	10	<b>38</b>	<b>19</b>	<b>45.5</b>	<b>EPMA; [LMV this study]</b>	
GOR132-G*	22	2	1.8	0.2	6.2	1	45.5	SIMS; [1]
			50	50	30	30		EPMA; [1]
					50	75		EPMA; [1]
	<d.l.		5.7	0.2	30	0.6		SIMS; [WHOI this study]
	<d.l.		<b>5.8</b>	<b>0.3</b>	<b>27</b>	<b>1.0</b>		<b>SIMS; [eq. 6, this study]</b>
4	8	11	13	<b>24</b>	<b>17</b>	<b>44.3</b>	<b>EPMA; [LMV this study]</b>	
VG2*, aka USNM 111240/52	334	14					50.6	SIMS; [4]
			1348	124	291	104		EPMA; [5]
			1365	58	316	38		EPMA; [5]
			1340	160				EPMA; [6]
			1305	135				EPMA; [7]
		1200	160	270	80		EPMA; [8]	

			1416	72	303	112		EPMA; [9]
			1500					EPMA; [10]
	243	36	1441	55	325	15		SIMS; [WHOI this study]
	<b>223</b>	<b>26</b>	<b>1352</b>	<b>66</b>	<b>249</b>	<b>28</b>		<b>SIMS; [eq. 6, this study]</b>
	<i>210</i>	<i>66</i>	<b>1343</b>	<b>23</b>	<b>306</b>	<b>13</b>		<b>EPMA; [LMV this study]</b>
VG-A99*, aka A99, USNM 113498/1			170	60				EPMA; [6]
			135	100	229	80		EPMA; [5]
	765	158	220	48	227	40		EPMA; [5]
			177	42	212	62		EPMA; [9]
			96	63				EPMA; [7]
			200	100				EPMA; [11]
	709	47					51.1	SIMS; [4]
	976	8						EPMA; [12]
			175	116	205	60		EPMA; [13]
	799	104	141	5	220	10		SIMS; [WHOI this study]
<b>734</b>	<b>76</b>	<b>132</b>	<b>6</b>	<b>170</b>	<b>18</b>		<b>SIMS; [eq. 6, this study]</b>	
<b>597</b>	<b>49</b>	<b>130</b>	<b>11</b>	<b>210</b>	<b>10</b>		<b>EPMA; [LMV this study]</b>	
Sletta	<b>3306</b>	<b>340</b>	<b>28</b>	<b>18</b>	<b>2075</b>	<b>64</b>		<b>EPMA; [LMV this study]</b>
KL2-G*	177	28	7.7	1.3	22.4	4.5	50.3	SIMS; [1]
			90	54	40	32		EPMA; [1]
			320	320	60	18		EPMA; [1]
	114;101;128	2;2;4						EPMA, SIMS, PIGE; [2]
	114	20	9.1	0.3	45	1		SIMS; [WHOI this study]
	<b>104</b>	<b>14</b>	<b>8.9</b>	<b>0.3</b>	<b>38</b>	<b>2</b>		<b>SIMS; [eq. 6, this study]</b>
99	154	23	15	51	23	50.5	EPMA; [LMV this study]	
<71				<324				ERDA; [Zurich this study]
ATHO-G*	770				530		74.5	EPMA; [14]
	0.7	0.07	0.6	0.07	2430	0	75.6	SIMS; [1]
			50	50	570	114		EPMA; [1]
			200	140	510	102		EPMA; [1]
	900	900	240	240	400	160		EPMA; [1]
	1464	186	4.8	0.2	681	32		SIMS; [WHOI this study]
	<b>637</b>	<b>137</b>	<b>4.4</b>	<b>0.4</b>	<b>512</b>	<b>60</b>		<b>SIMS; [eq. 6, this study]</b>
	<b>668</b>	<b>204</b>	<i>17</i>	<i>12</i>	<b>453</b>	<b>22</b>	<b>74.1</b>	<b>EPMA; [LMV this study]</b>
<b>637</b>	<b>158</b>			<b>334</b>	<b>196</b>		<b>ERDA; [Zurich this study]</b>	
KE12*	4338	1096						EPMA; [15]
	4400							EPMA; [15]
					3270	110	70.8	EPMA; [16]
	4200				3300			EPMA; [16]
	4000	240						Selective ion method; [17]
					3225	160		EPMA; [18]
					3200	800		EPMA; [19]
	4513	88						EPMA; [12]
	7537	932	290	11	4668	226		SIMS; [WHOI this study]
	<b>3898</b>	<b>689</b>	<b>208</b>	<b>13</b>	<b>3483</b>	<b>423</b>		<b>SIMS; [eq. 6, this study]</b>
<b>4488</b>	<b>151</b>	<b>150</b>	<b>14</b>	<b>3414</b>	<b>55</b>		<b>EPMA; [LMV this study]</b>	

	<b>3848</b>	<b>230</b>			<b>3483</b>	<b>400</b>		<b>ERDA; [Zurich this study]</b>
Alvin 2390-5	630	44			241	19		SIMS; [20]
	<b>303</b>	<b>35</b>	<b>1270</b>	<b>9</b>	<b>358</b>	<b>5</b>	<b>49</b>	<b>EPMA; [LMV this study]</b>
Alvin 2746-15	<b>123</b>	<b>2</b>	<b>1449</b>	<b>15</b>	<b>890</b>	<b>9</b>	<b>50</b>	<b>EPMA; [LMV this study]</b>

[1] Jochum et al. 2006; [2] Guggino and Hervig, 2010; [3] Diaz et al. 2006; [4] Straub & Layne 2003; [5] Thordasson et al. 1996; [6] Dixon et al. 1991; [7] Thornber et al., 2002; [8] Coombs et al. 2004; [9] DeHoog et al. 2001; [10] Hall et al. 2006; [11] Fisk & Kelley 2002; [12] Witter & Kuehner, 2004; [13] Streck & Wacaster 2006; [14] Oskarsson et al. 1982; [15] Palais and Sigurdsson, 1989; [16] Métrich & Rutherford, 1991; [17] Mosbah et al, 1991; [18] Marianelli et al. 1995; [19] Cioni et al. 1998. [20] Le Roux et al., 2006. <d.l. means below detection limit. Numbers in *italic* are considered below detection limit.

Table 3: Result of error weighted regression of Eq. 5, and Eq. 6

	ak/dk	±	bk/ck	±	Intercept*	±	RRM**
F (Eq. 5)	682	27	-5.0	0.5	-47	38	0.05
F (Eq. 6)	17.8	0.8	-0.185	0.002	-47	38	0.04
S (Eq. 5)	400	11	4.46	0.03	3.3	20	0.42
S (Eq. 6)	19.8	0.6	-0.1466	0.0001	3.3	20	0.23
Cl (Eq. 5)	14.0	13.6	12.1	0.2	19	17	0.49
Cl (Eq. 6)	12.7	1.5	-0.0057	0.0005	19	17	0.47

\* Intercept values are taken from the working curves of Fig. 2. This choice was to reduce cases of erroneous fit coefficients. \*\*RRMS : Reduced residual mean-square value, in which residual of fit values were normalized by the uncertainty of the standards, and the mean value of the sum of the square is reported. When RRMS > 1 indicates that fitted values on average plot outside of 1 sigma of the standard value.

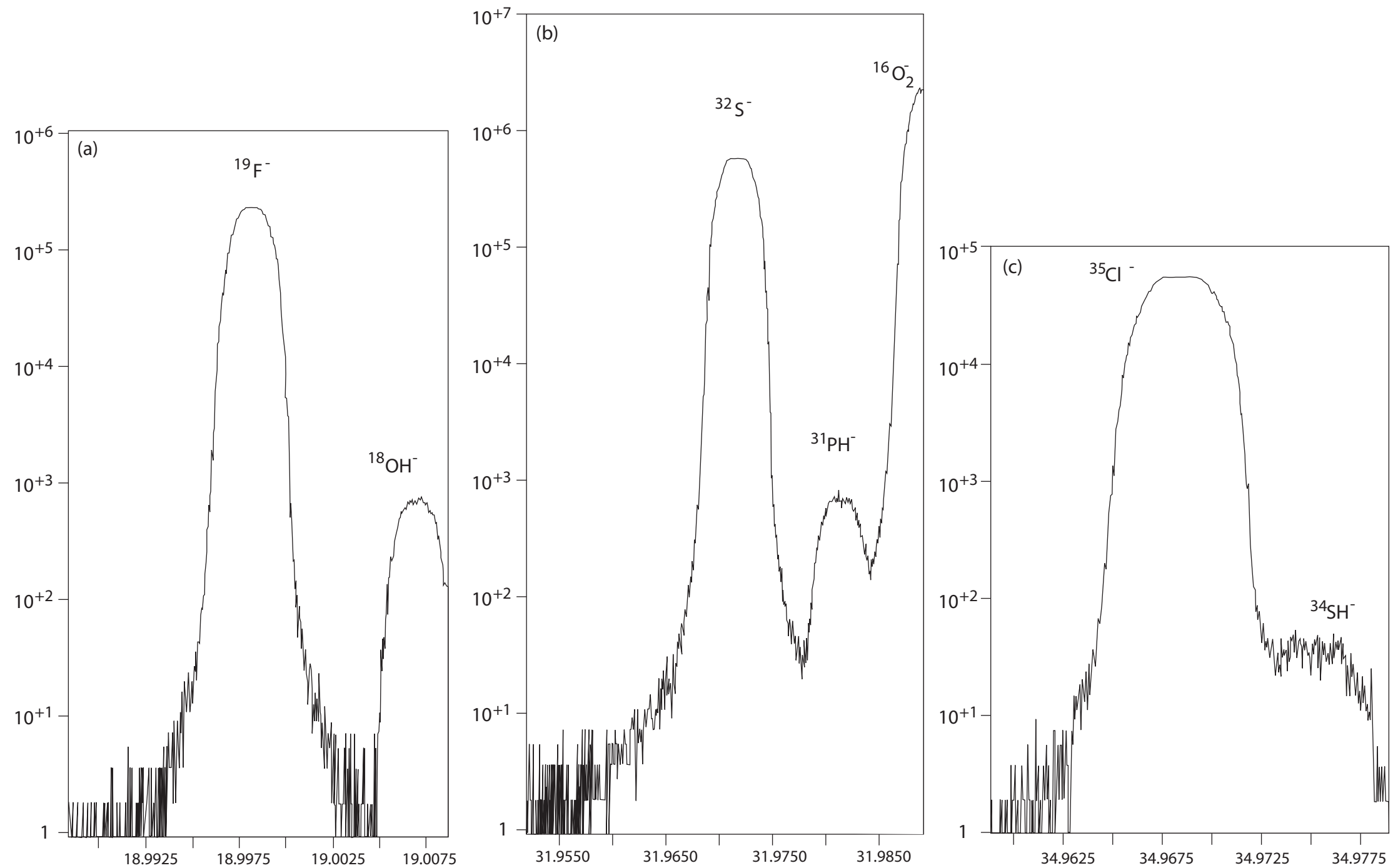
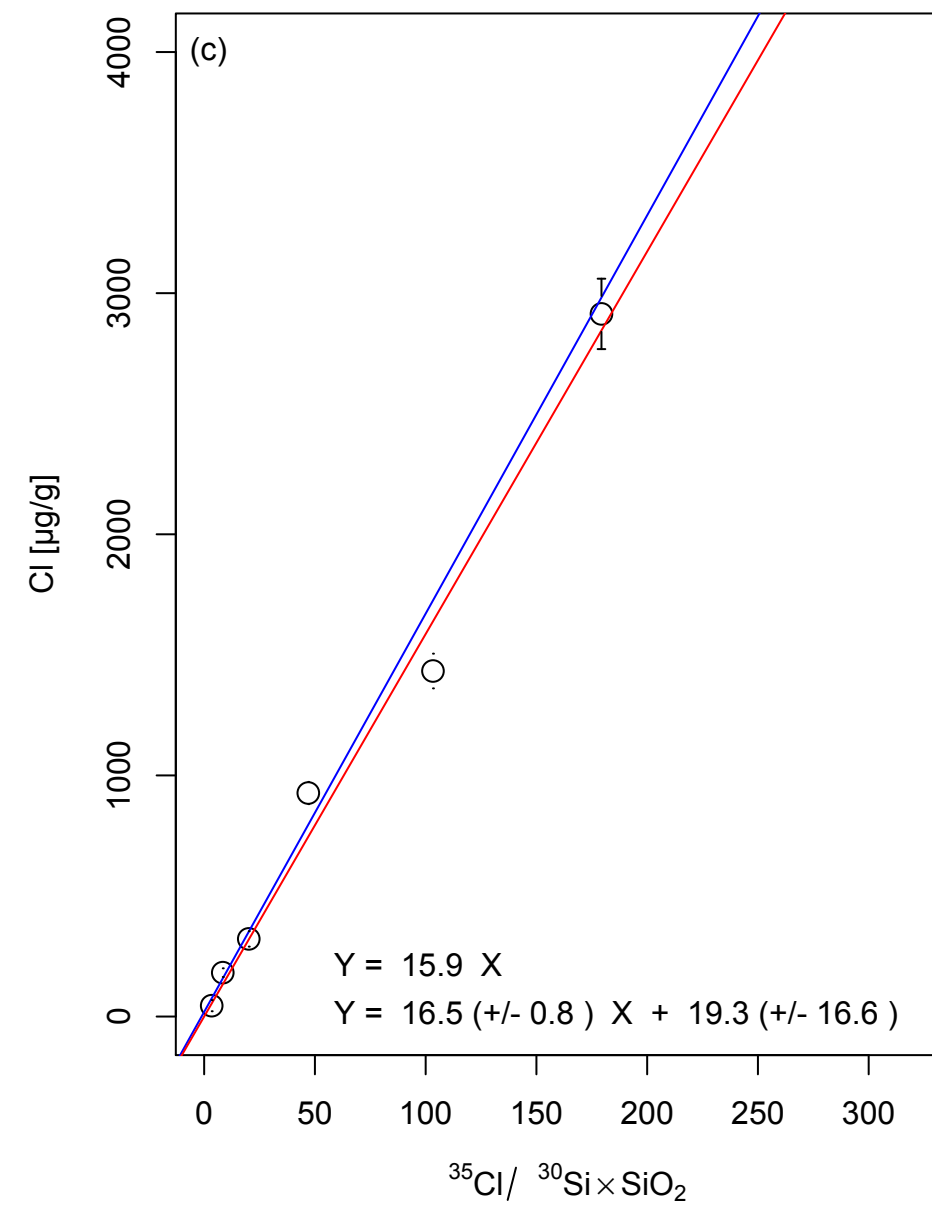
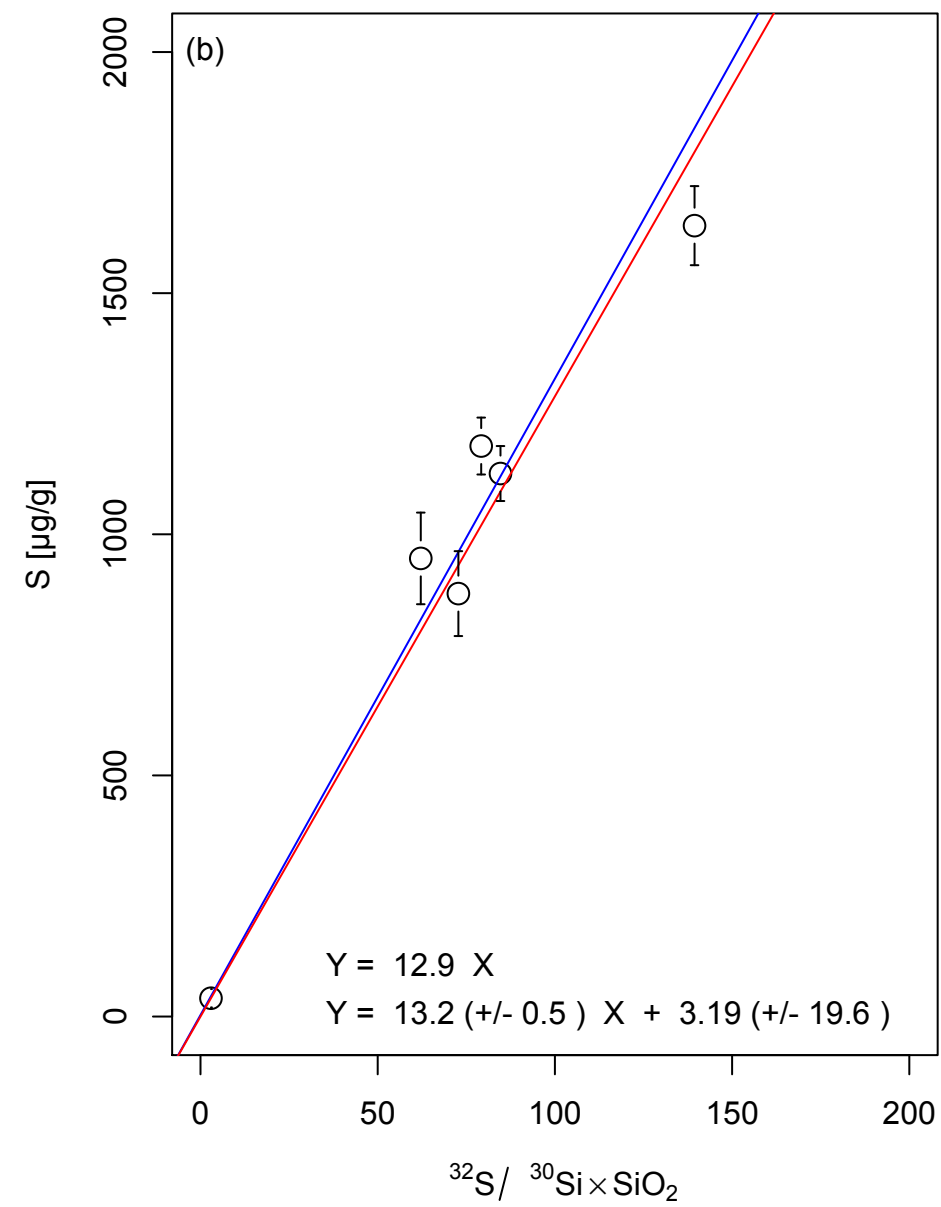
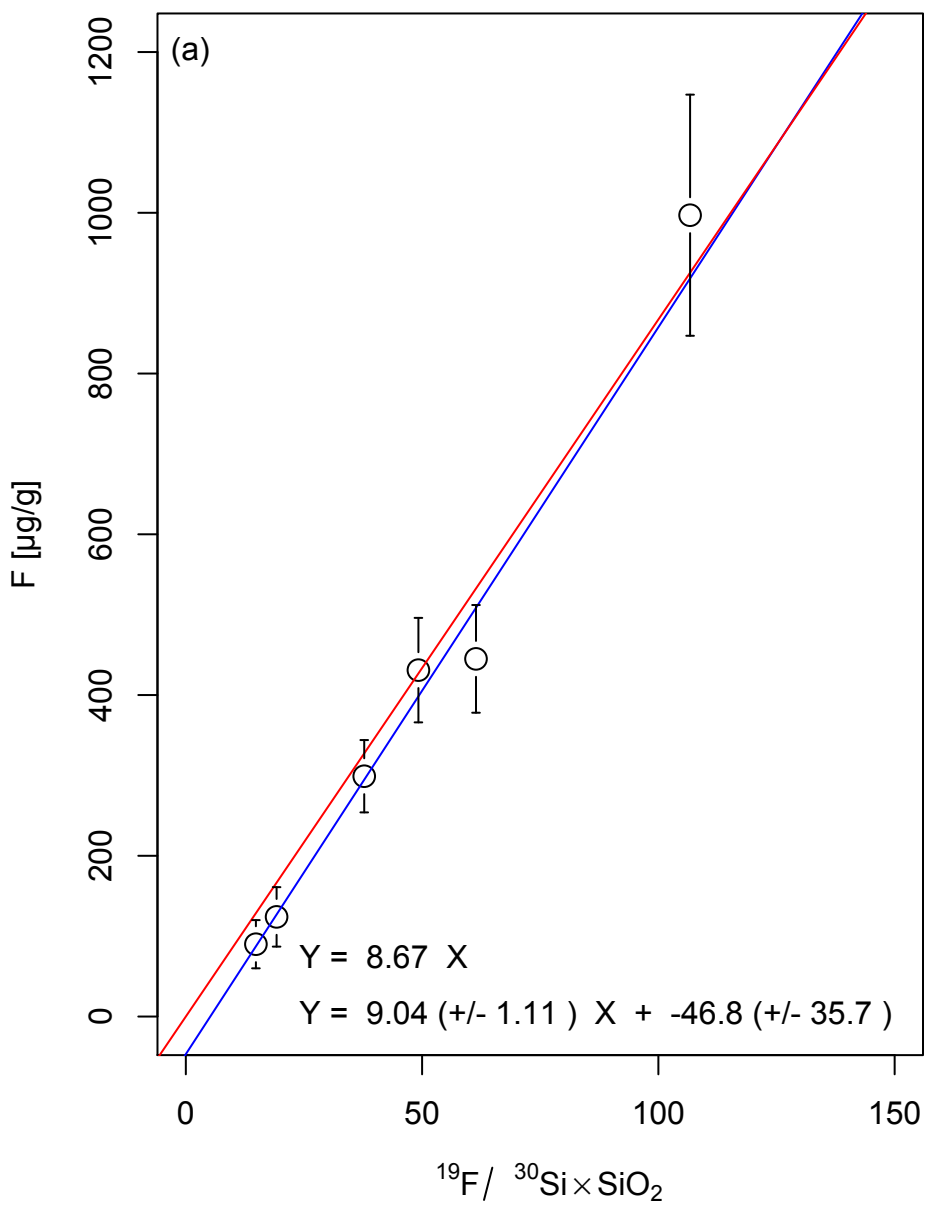


Fig. 1



**Fig. 2**

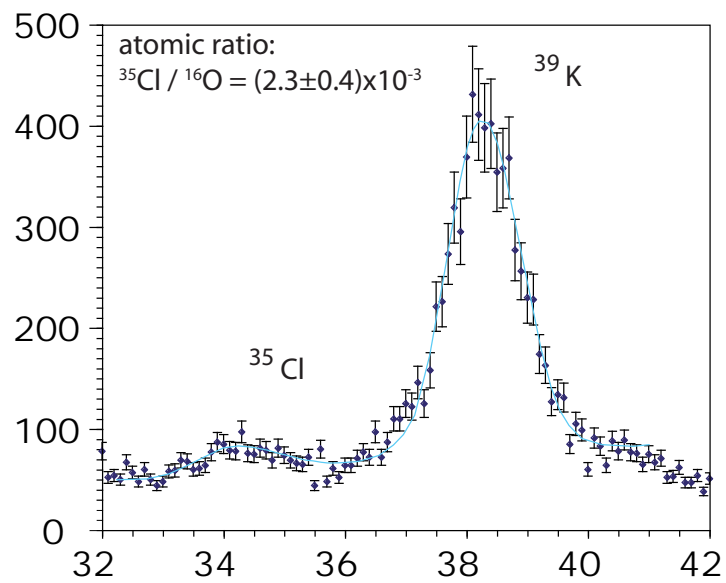
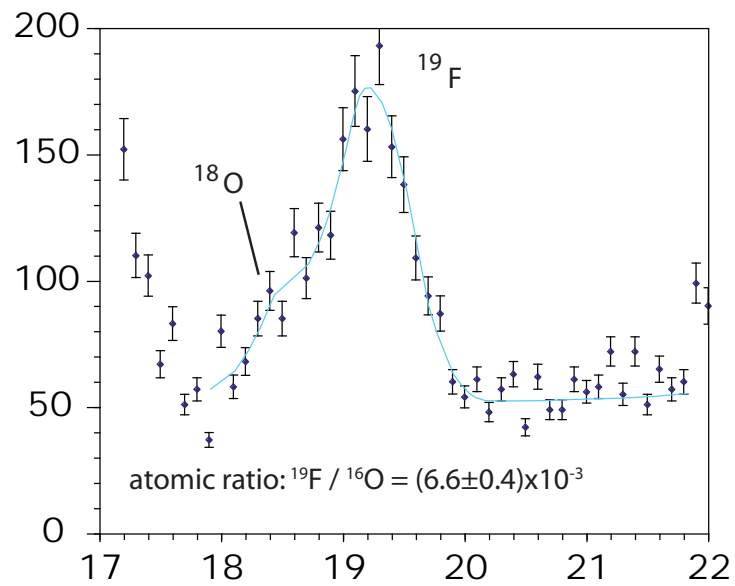
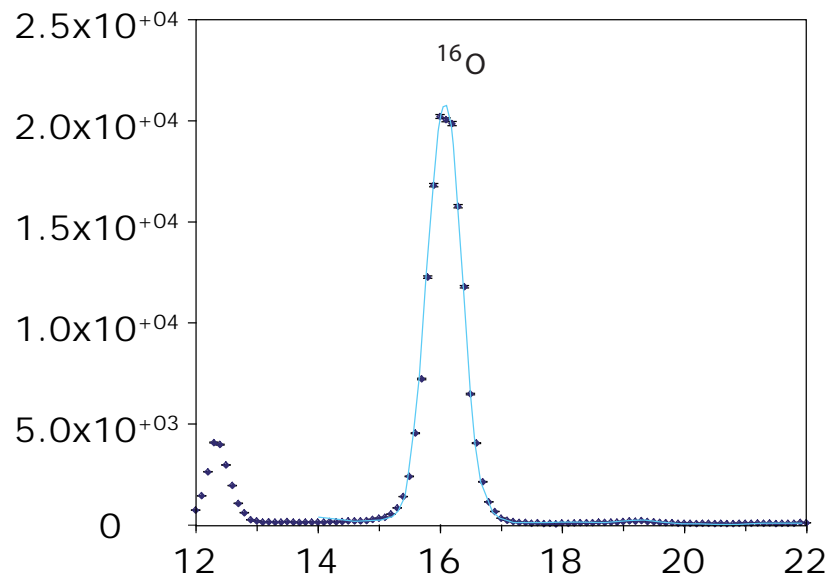


Fig. 3

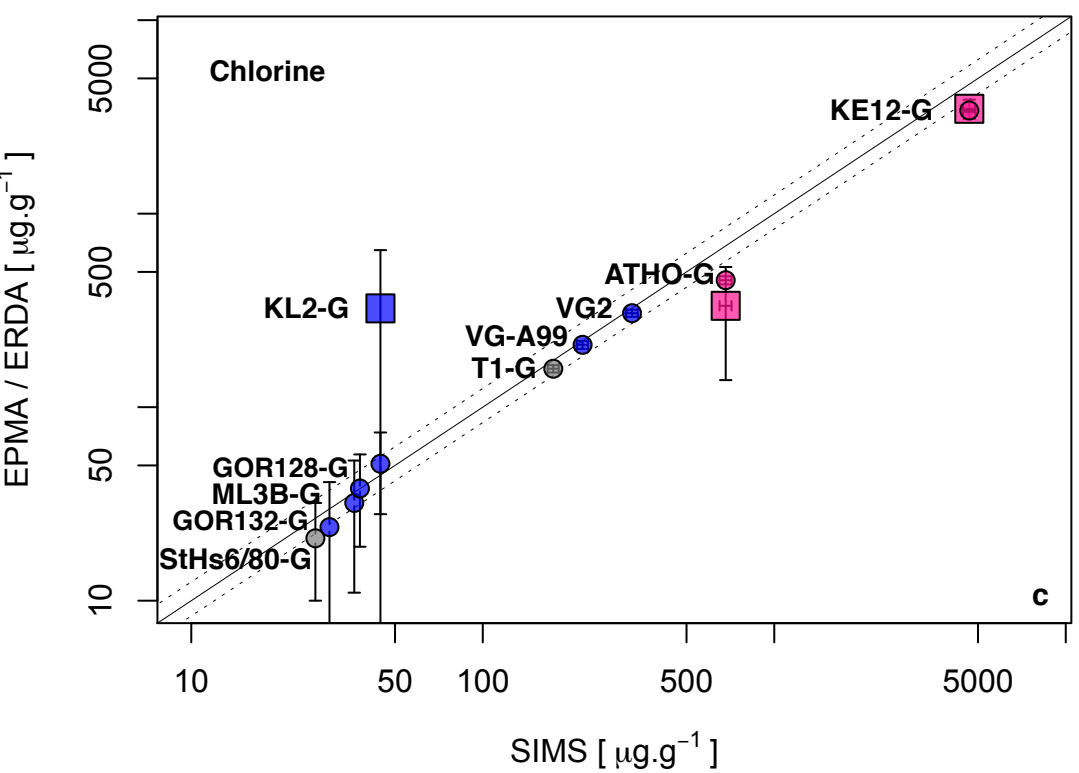
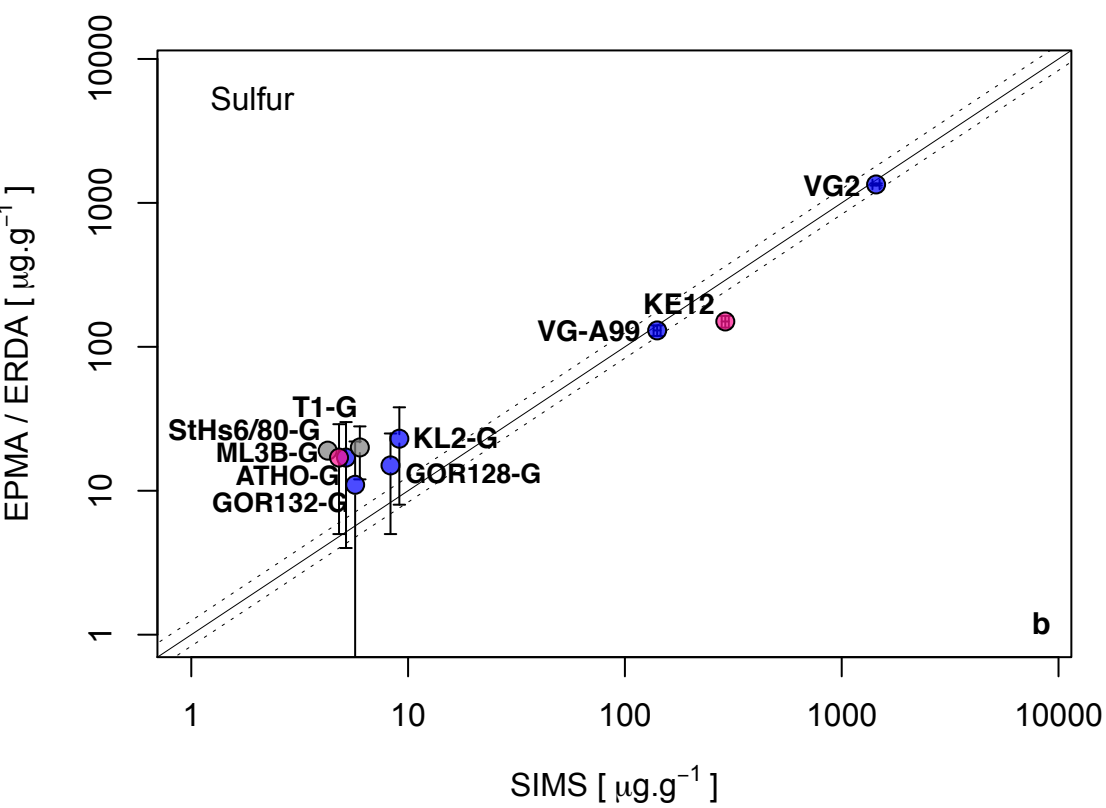
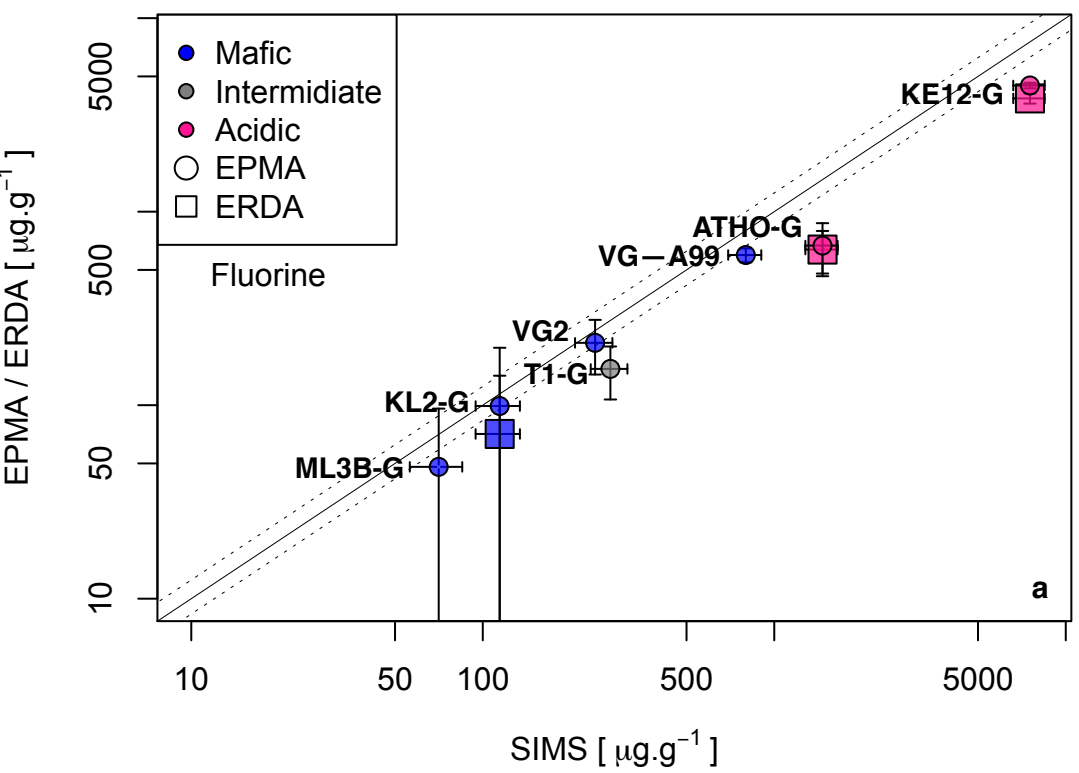
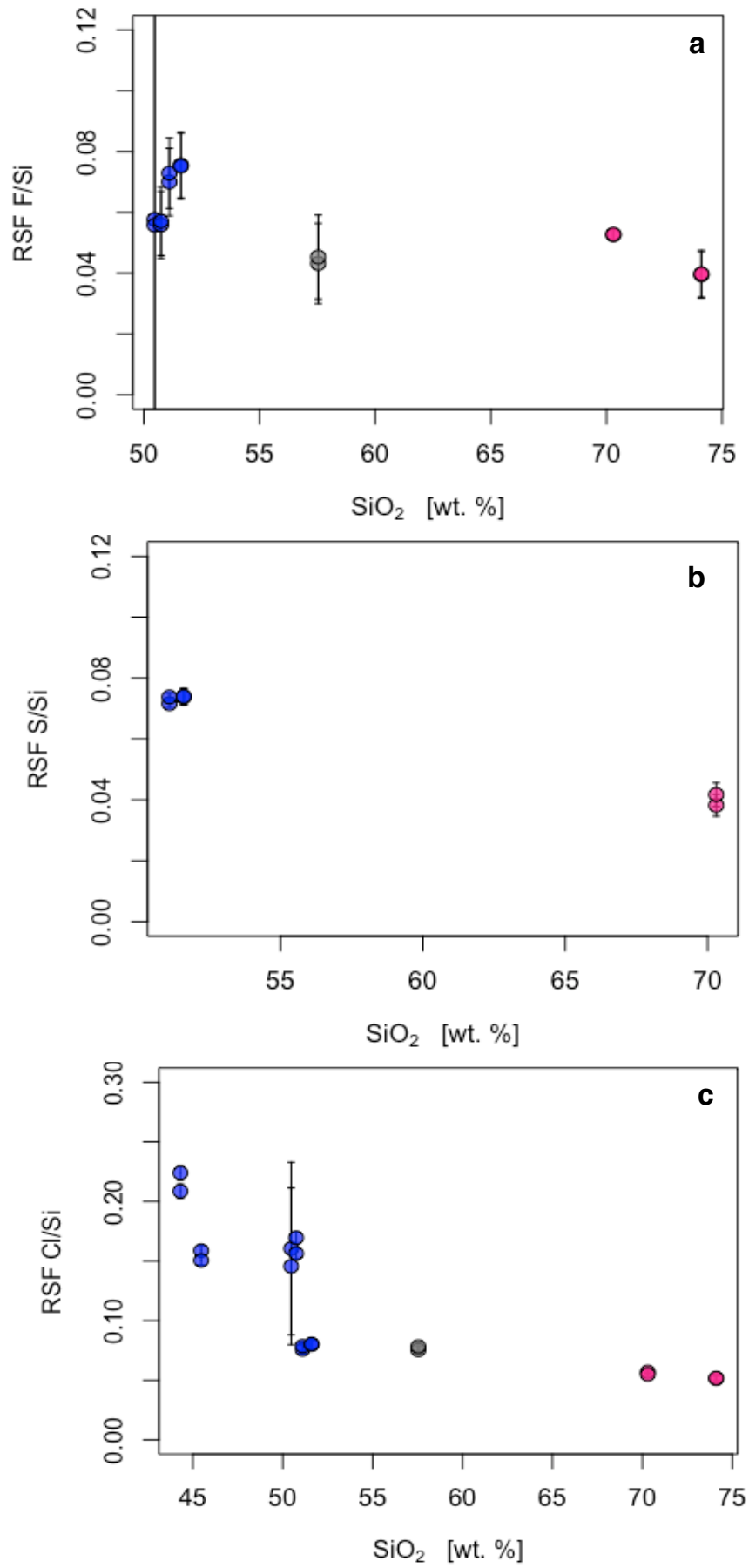


Fig. 4



**Fig. 5**

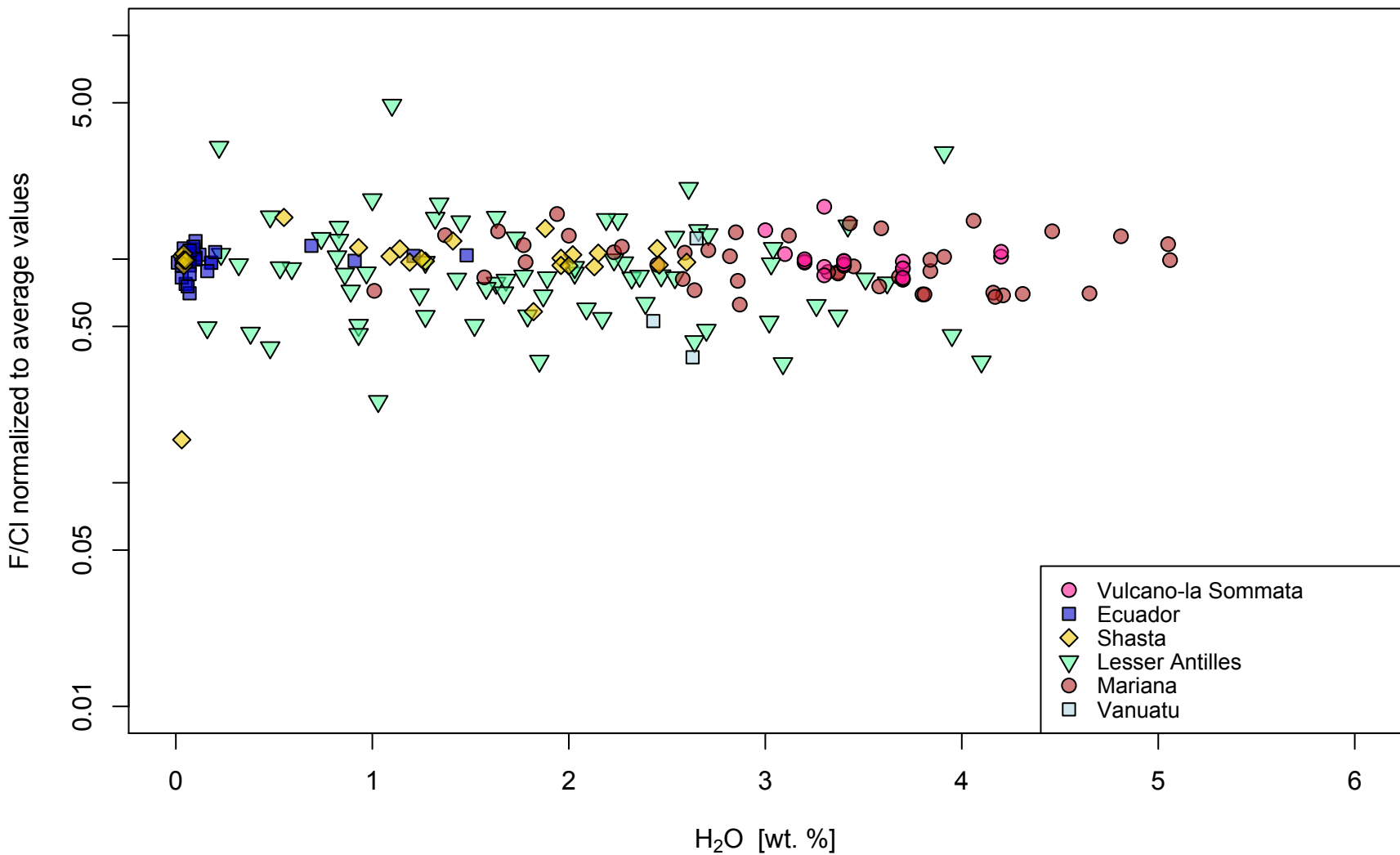


Fig. 6